Eur. J. Mineral.
2019, **31**, 389–397
Published online 17 October 2018

The rockbridgeite group approved and a new member, ferrorockbridgeite, $(Fe^{2+},Mn^{2+})_2(Fe^{3+})_3(PO_4)_3(OH)_4(H_2O)$, described from the Hagendorf Süd pegmatite, Oberpfalz, Bavaria

Ian E. GREY[1,*], Anthony R. KAMPF[2], Erich KECK[3], John D. CASHION[4], Colin M. MacRAE[1], Yesim GOZUKARA[5], Vanessa K. PETERSON[6] and Finlay L. SHANKS[7]

[1]CSIRO Mineral Resources, Private Bag 10, Clayton South, Victoria 3169, Australia
*Corresponding author, e-mail: Ian.grey@csiro.au
[2]Mineral Sciences Dept, Natural History Museum of Los Angeles County, 900 Exposition Boulevard, Los Angeles, CA 90007, USA
[3]Algunderweg 3, 92694 Etzenricht, Germany
[4]School of Physics and Astronomy, Monash University, Victoria 3800, Australia
[5]CSIRO Manufacturing, Private Bag 10, Clayton South, Victoria 3169, Australia
[6]Australian Centre for Neutron Scattering, Australian Nuclear Science and Technology Organisation, Locked Bag 2001, Kirrawee DC, New South Wales 2232, Australia
[7]School of Chemistry, Monash University, Clayton, Victoria 3800, Australia

Abstract: The rockbridgeite group has been officially established by the IMA Commission on New Minerals, Nomenclature and Classification. The general formula is based on the structure and is $A_2B_3(PO_4)_3(OH, H_2O)_5$, where A = the octahedrally coordinated $M2$ site, in which divalent cations are ordered, and B = the octahedrally coordinated $M1$ + $M3$ sites, which contain predominantly Fe^{3+}, with trace Al. The different rockbridgeite-group minerals are distinguished by the occupancy of the A site. The ideal formula for rockbridgeite is $\left(Fe^{2+}_{0.5}Fe^{3+}_{0.5}\right)_2Fe^{3+}_3(PO_4)_3(OH)_5$, that for frondelite is $\left(Mn^{2+}_{0.5}Fe^{3+}_{0.5}\right)^2Fe^{3+}_3(PO_4)_3(OH)_5$ and that for plimerite is $Zn_2Fe^{3+}_3(PO_4)_3(OH)_4(H_2O)$. In order to preserve the identity of frondelite and rockbridgeite within the structure-based formalism, these species correspond to mid-series compositions. We describe here the new end-member, ferrorockbridgeite, with dominant Fe^{2+} in the A site, from the Hagendorf Süd pegmatite mine, Oberpfalz, Bavaria. Electron microprobe analyses, coupled with Mössbauer spectroscopy, gives the empirical formula $Fe^{2+}_{1.33}Mn^{2+}_{0.52}Zn_{0.03}Ca_{0.05}Fe^{3+}_{3.03}Al_{0.01}P_{2.97}H_{6.17}O_{17}$. The simplified formula is $(Fe^{2+},Mn^{2+})_2Fe^{3+}_3(PO_4)_3(OH)_4(H_2O)$. Ferrorockbridgeite is orthorhombic, space group *Bbmm*, with a = 13.9880(4), b = 16.9026(5), c = 5.1816(1) Å, V = 1225.1 Å^3 and Z = 4. The six strongest lines in the X-ray powder diffraction pattern are [d_{meas}/Å (I) (*hkl*)]: 4.853 (26) (101), 3.615 (24) (240), 3.465 (33) (301), 3.424 (39) (410), 3.205 (100) (321) and 1.603 (24) (642). Optically, ferrorockbridgeite is biaxial (–) with α = 1.763(3), β = 1.781(calc), γ = 1.797(3) (white light) and $2V$ (meas.) = 87(1)° from extinction data. The optical orientation is X = **c**, Y = **a**, Z = **b**. The pleochroism is X = blue green, Y = olive green, Z = yellow brown; $X \approx Y > Z$.

Key-words: rockbridgeite group; nomenclature; ferrorockbridgeite; new mineral; crystal structure; neutron diffraction; iron phosphate.

1. Introduction

Rockbridgeite was first described by Frondel (1949) as a new mixed-valency iron phosphate mineral, with a powder X-ray diffraction pattern distinct from that for dufrenite, with which it had been confused ''since earliest times''. Frondel gave the formula for rockbridgeite as $Fe^{2+}Fe^{3+}_6(PO_4)_4(OH)_8$. Lindberg (1949) applied single-crystal diffraction methods to determine that rockbridgeite had *B*-centred orthorhombic symmetry, with cell parameters a = 13.89, b = 17.01, c = 5.21 Å. From new chemical analyses, combined with the unit-cell data, Lindberg obtained the revised rockbridgeite formula $Fe^{2+}Fe^{3+}_4(PO_4)_3(OH)_5$, and characterized a manganese analogue, frondelite, $Mn^{2+}Fe^{3+}_4(PO_4)_3(OH)_5$. Elliott *et al*. (2009) described a zinc-dominant analogue from Broken Hill, plimerite, and proposed that its composition conformed to the general formula $AB_4(PO_4)_3(OH)_5$ with A = divalent cations (Zn, Mn^{2+}, Fe^{2+}) and B = trivalent cations (Fe^{3+}, Al). The use of this formula for plimerite was criticized by Sejkora *et al*. (2011) because the analyses of Elliott *et al*. (2009) gave closer to two atoms per formula unit (*apfu*) of divalent cations. More specifically, the formula $AB_4(PO_4)_3(OH)_5$ is not consistent with the crystal structure.

The crystal structure of rockbridgeite was solved by Moore (1970) in space group *Bbmm*. Moore's (1970) study showed that the structural formula for minerals with the

0935-1221/19/0031-2823 $ 4.05
https://doi.org/10.1127/ejm/2019/0031-2823

rockbridgeite structure is $M1(M2)_2(M3)_2(PO_4)_3(OH, H_2O)_5$. A number of recent high-quality single-crystal structure refinements have confirmed that the sites *M*1 and *M*3 contain predominantly Fe^{3+} (with minor Al), whereas divalent cations are ordered at the *M*2 site (Redhammer *et al.*, 2006; Elliott *et al.*, 2009; Röska *et al.*, 2018; Grey *et al.*, 2018a). On this basis, we proposed a new structure-based formula for rockbridgeite-group minerals, $A_2B_3(PO_4)_3(OH, H_2O)_5$, which has been approved by the IMA Commission on New Minerals, Nomenclature and Classification (CNMNC). *A* corresponds to the *M*2 site and contains all divalent cations, while *B* = *M*1 + *M*3 and contains predominantly Fe^{3+}. The different rockbridgeite-group minerals are distinguished by the occupancy of the *A* site. Rockbridgeite is ideally $(Fe^{2+}_{0.5}Fe^{3+}_{0.5})_2Fe^{3+}_3(PO_4)_3(OH)_5$, and frondelite is $(Mn^{2+}_{0.5}Fe^{3+}_{0.5})_2Fe^{3+}_3(PO_4)_3(OH)_5$. Plimerite, with ideally two Zn *apfu*, requires replacement of one hydroxyl ion by H_2O for charge balance, giving $Zn_2Fe^{3+}_3(PO_4)_3(OH)_4(H_2O)$. The substitution of H_2O for OH in a rockbridgeite-group mineral containing predominantly divalent cations in the *A* site has recently been confirmed by Röska *et al.* (2018) using neutron diffraction.

In order to preserve the compositional identity of rockbridgeite and frondelite within the structure-based formalism, the phase-composition diagram defined by occupation of the *A* site by Fe^{2+}, Mn^{2+} and Fe^{3+} is divided into five compositional phase-fields rather than the usual three fields, as illustrated in Fig. 1. We have chosen this approach because the published analyses for type frondelite and type rockbridgeite (Lindberg, 1949), when plotted according to the structural formula in Fig. 1, both have considerably more than 50% Fe^{3+} in the *A* site, and so both minerals would be classed as ''ferrirockbridgeite'', if the normal ternary phase boundaries were used. This would lead to the unfortunate situation of having to discredit one of these well-entrenched species, which are also valuable indicators of phosphate paragenetic environments. In the five-field diagram, the ideal rockbridgeite and frondelite compositions correspond to mid-series compositions rather than end-member compositions. Such a scheme involves the eventual characterization of three new rockbridgeite-group members with dominant Fe^{2+}, Mn^{2+} and Fe^{3+} in the *A* site. In this paper, we report the characterisation of ferrorockbridgeite as the member with dominant Fe^{2+} in the *A* site. The mineral and its name have been approved by the IMA CNMNC, IMA2018-004 (Grey *et al.*, 2018b).

Measurements were made on two hand-specimens, IGC29 and IGC90 (Fig. 1). Only the latter sample had large-enough regions of pure ferrorockbridgeite to provide a 5 g sample for neutron powder diffraction. Other measurements including single-crystal and powder XRD, Mössbauer spectroscopy, thermal analyses and optical measurements were made on both samples and are reported here. The two specimens are housed in the mineralogical collections at Museum Victoria, registration number M54126. A small fragment removed from specimen IGC29 is deposited in the collections of the Natural History Museum of Los Angeles County, catalogue number 67281.

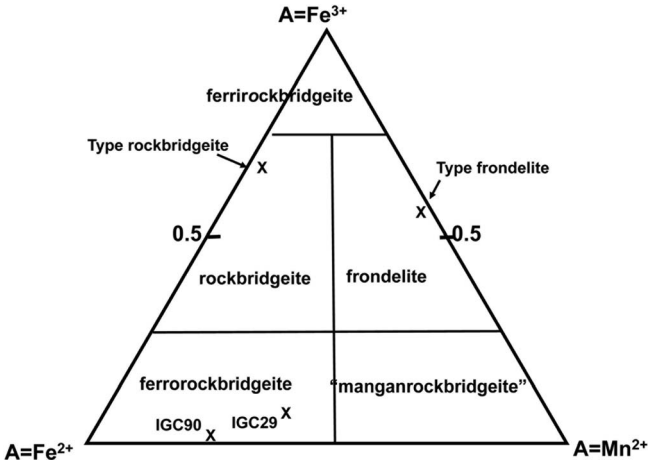

Fig. 1. Rockbridgeite-group mineral phase fields, based on the occupation of the *M*2 site (= *A*). Analysis points for two ferrorockbridgeite samples shown, as well as for type frondelite and type rockbridgeite from Lindberg (1948).

2. Occurrence, mineral assemblage and paragenesis

Ferrorockbridgeite was found in specimens collected by one of the authors (EK) from the 76 m level of the Hagendorf-Süd pegmatite mine, Hagendorf, a branch of Amberger Kaolinwerke (AKW), Hirschau, Oberpfalz, Bavaria, Germany (49°39′1″N, 12°27′35″E). It forms as densely packed, lustrous, black blades, associated with oxidized schoonerite-group minerals, jahnsite, idiomorphic crystals of laueite and coatings of mitridatite.

According to Mücke's (1981) paragenetic classification for phosphate minerals at Hagendorf Süd, ferrorockbridgeite belongs to his category II of secondary phosphates involving rockbridgeite. It has most likely formed from hydrothermal alteration of triphylite as well as from zwieselite.

3. Physical properties

Ferrorockbridgeite occurs as compact intergrowths of dark green to black blades, shown in Fig. 2. Individual blades have lengths up to 2 mm and are on the order of 10 μm thick. The ferrorockbridgeite blades are flattened on {010} and elongated on [001]. The density, measured using a Berman balance with toluene is 3.21(1) g cm^{-3} for IGC29 and 3.33(1) g cm^{-3} for IGC90, whereas the calculated density, based on the empirical formula and X-ray powder diffraction, is 3.51 g cm^{-3}. The lower measured density is attributed to the presence of sub-micrometer scale porosity that is not penetrated by the density liquid. The ultrafine-scale porosity is shown in Fig. 3.

Optically, ferrorockbridgeite is biaxial (–), with the indices of refraction for IGC29 $\alpha = 1.763(3)$, $\beta = 1.781$(calc), $\gamma = 1.797(3)$ (measured in white light). The measured $2V$ is 87(1)° from extinction data using EXCALIBR (Gunter *et al.*, 2004). β could not be measured because of

Fig. 2. Hand specimen IGC-29. Ferrorockbridgeite shown by green arrow. Field of view 6 mm.

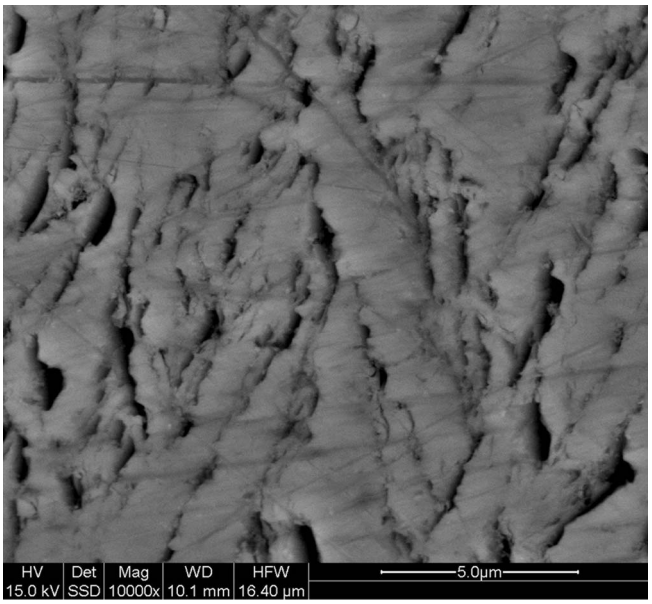

Fig. 3. Back-scattered electron image of sectioned and polished ferrorockbridgeite (IGC29), showing fine-scale porosity.

its unfavorable orientation perpendicular to the thin direction of the blades. Consequently, β was calculated from α, γ and 2*V*. For IGC90, α = 1.758(3), β = 1.777(calc), γ = 1.797(3) and 2*V*(meas) = 89.8(5), within one standard deviation of the values for IGC29.

The dispersion is strong, based upon extinction colors; but the sense could not be determined because the isogyres could not be observed. The optical orientation is *X* = **c**, *Y* = **a**, *Z* = **b**. The pleochroism is *X* = blue green, *Y* = olive green, *Z* = yellow brown; $X \approx Y > Z$. The Gladstone-Dale compatibility (Mandarino, 1981) $1 - (K_P/K_C) = 0.048$ (good), based on the empirical formula with the measured density and optical properties for IGC29. The measured density was used rather than the calculated density to take account of the fine-scale porosity of the crystals (Fig. 3), which decreases the measured indices of refraction similarly to the measured density.

4. Mössbauer spectroscopy

The Mössbauer spectrum for ferrorockbridgeite in sample IGC90 was taken using a conventional constant acceleration drive with a symmetrical sawtooth waveform (Wissel). The source of ^{57}Co in rhodium was maintained at room temperature. The spectrum was fitted with four Lorentzian doublets (two each for Fe^{3+} and for Fe^{2}) and also using five Lorentzian doublets (three for Fe^{3+} and two for Fe^{2}). The fitting parameters are reported in Table 1. The isomer shifts are given relative to α–Fe at room temperature. The four-doublet fit gave parameters close to those reported by Redhammer *et al.* (2006) for manganese-bearing rockbridgeite from Hagendorf (these authors additionally allocated a small doublet contribution (area = 3%) to Fe^{3+} in the *M*2 site). The fit index, however, was very high, with $\chi^2 = 2.28$.

Allowing a third ferric doublet in the fitting gave a marked reduction in χ^2 to 0.86. The fitted spectrum is shown in Fig. 4. The site assignments given in Table 1 are based on the crystal-structure refinement, which gives 1 Fe^{3+}, 1.2 Fe^{2+} and 2 Fe^{3+} per formula unit in the sites *M*1, *M*2 and *M*3, respectively. The two separate doublets assigned to the *M*3 site, with different QS values, are considered to result from next-nearest-neighbor effects due to different local distributions of Fe^{3+} and vacancies in the half-occupied *M*3 sites. Splitting of the peaks corresponding to Fe^{2+} in the *M*2 site into two doublets is also considered to be due to next-nearest-neighbor effects since the *M*2 site contains a mix of Mn^{2+} and Fe^{2+} cations. The *M*2 site Fe^{2+} Mössbauer parameters are close to those reported by Redhammer *et al.* (2006). The ratio of the ferrous-to-ferric doublet areas for the five-Lorentzian fit gives 30.6% Fe^{2+} to 69.4% Fe^{3+}. Applying the same procedure to the Mössbauer spectrum for ferrorockbridgeite in sample IGC29 gave a ratio of ferrous-to-ferric doublet areas of 26% Fe^{2+} to 74% Fe^{3+}.

5. Thermal analysis

The H_2O content was measured by thermogravimetric analysis, performed on 26 mg ground samples of IGC29 and IGC90 using a Netzsch STA 449 F1 Jupiter Simultaneous TGA/DSC thermal analyser. The analyses were performed in nitrogen, with a ramp rate of 10 °C/min, between 30 and 800 °C. Evolved-gas analysis was made using a coupled Thermostar Pfeiffer mass spectrometer (MS). The MS showed that H_2O evolution occurred up to 600 °C (see Fig. 5). The mass loss to 600° was 10.0 wt% for both samples. This is 1.5 wt% higher than the expected mass loss due to H_2O evolution based on the crystal-structure. A possible explanation is the presence of non-structural water in enclosed micropores in the mineral.

Table 1. Mössbauer parameters for ferrorockbridgeite sample IGC90. Isomer shift δ, quadrupole splitting Δ, half-width-half-maximum (HWHM) and area of doublet *A*.

δ (mm/s)	Δ (mm/s)	HWHM (mm/s)	*A* (%)	Atoms per formula	Assignment
4-Lorentzian fit, χ^2 = 2.28					
0.40(1)	0.48(1)	0.166(2)	51.9	2.30	Fe^{3+} in *M*3
0.47(1)	0.79(1)	0.153(4)	18.6	0.82	Fe^{3+} in *M*1
1.07(1)	3.09(1)	0.127(6)	10.4	0.46	Fe^{2+} in *M*2
1.13(1)	2.83(1)	0.181(6)	19.1	0.85	Fe^{2+} in *M*2
5-Lorentzian fit, χ^2 = 0.86					
0.37(1)	0.42(1)	0.124(6)	19.7	0.87	Fe^{3+} in *M*3
0.38(1)	0.63(1)	0.141(5)	28.6	1.26	Fe^{3+} in *M*3
0.55(1)	0.65(1)	0.174(6)	21.1	0.93	Fe^{3+} in *M*1
1.07(1)	3.10(1)	0.128(6)	10.4	0.46	Fe^{2+} in *M*2
1.13(1)	2.83(1)	0.183(6)	20.2	0.89	Fe^{2+} in *M*2

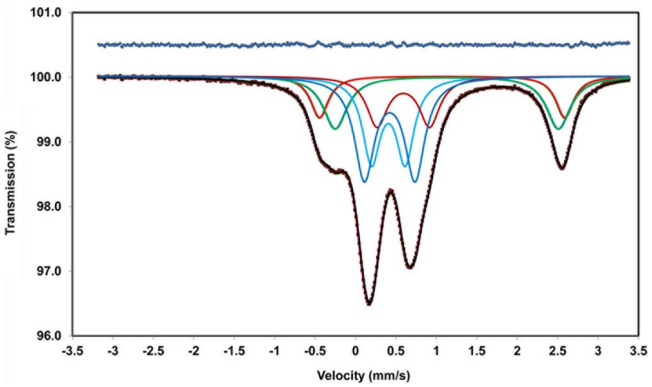

Fig. 4. Fitted Mössbauer spectrum for ferrorockbridgeite (specimen IGC90). The upper line is a difference plot.

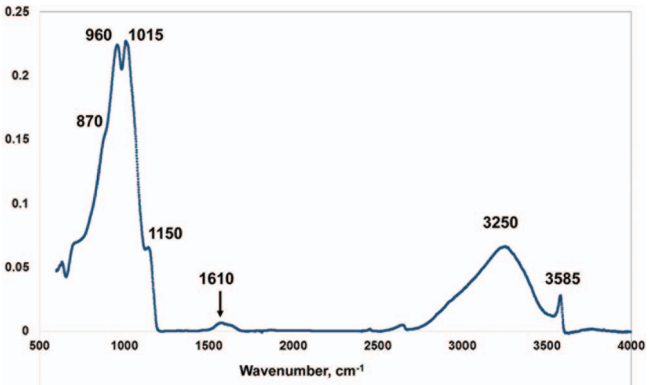

Fig. 6. Infrared spectrum for ferrorockbridgeite.

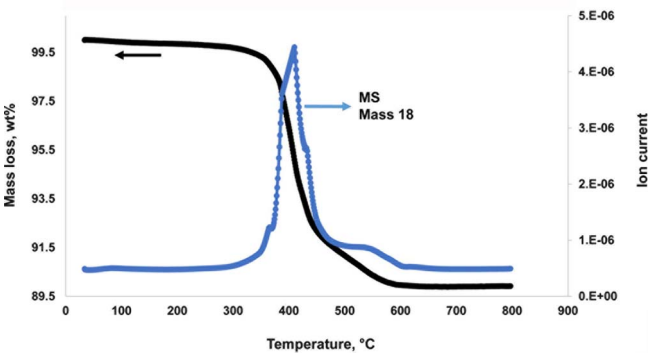

Fig. 5. Thermogravimetric curve and mass spectroscopy of evolved H_2O for ferrorockbridgeite.

6. Infrared spectroscopy

Attenuated total-reflection infrared spectroscopy on ground crystals of ferrorockbridgeite was conducted using a Bruker Equinox IFS55 spectrometer fitted with Judson MCT detector and Specac diamond ATR. One hundred co-added scans were employed at a spectral resolution of 4 cm^{-1}. The infrared spectrum is shown in Fig. 6. In the OH stretching region, a weak sharp peak at 3585 cm^{-1} is assigned to hydroxyl ion vibrations, while a broad peak at 3250 cm^{-1} is attributed to water molecules and strongly hydrogen-bonded hydroxyl ions. There is a corresponding H–O–H bending vibration for water molecules at ~1610 cm^{-1}. Four $(PO_4)^{3-}$ stretching vibrations, at 1150, 1015, 960 and 870 cm^{-1} are in similar positions to those reported for rockbridgeite from Hagendorf by Röska *et al.* (2018).

7. Chemical composition

Crystals of ferrorockbridgeite specimens IGC29 and IGC90 were analysed using wavelength dispersive spectrometry on a JEOL JXA 8500F Hyperprobe operated at an accelerating voltage of 15 kV and a beam current of 4 nA. The beam was defocused to 5 μm. Analytical results are given in Table 2. The FeO/Fe_2O_3 contents were determined by Mössbauer spectroscopy and the water contents are from the thermal analyses. The low electron microprobe (EMP) analysis total for IGC29 is most likely due to the presence of fine-scale porosity (Nasdala *et al.*, 2009), shown in Fig. 3. The original wet-chemical analyses on ferrorockbridgeite, performed by EK in 1957, are given in Table 2 for comparison. The high CaO content reflects some impurity phase contamination that inevitably resulted because of the high sample quantities required for the classical wet-chemical analyses. The empirical formulae from the EMP

Table 2. Analytical data (wt%) for ferrorockbridgeite.

	EMP results				IGC90	
	IGC90 (average of 30)			IGC29 (av. of 7)	wet-chemical	
	Mean	Range	SD	SD in parenthesis	EK analyst	Probe standard
ZnO	0.42	0.07–0.84	0.17	0.71(0.48)	n.a	Phosphophyllite
MnO	5.51	4.48–6.79	0.54	7.89(0.48)	6.29*	Rhodonite
MgO	0.02	0.0–0.13	0.03	0.0(0.07)	0.11	Spinel
CaO	0.40	0.18–0.58	0.10	0.39(0.14)	2.16	Wollastonite
Fe_{tot} as Fe_2O_3	(52.4)	49.1–54.5	1.3	48.8(1.4)		Hematite
FeO	14.74			11.4	12.0	
Fe_2O_3	36.4			36.1	37.6	
Al_2O_3	0.11	0.00–0.31	0.07	0.0	0.0	Berlinite
P_2O_5	31.6	29.1–35.7	1.2	30.9(0.4)	31.9	Berlinite
H_2O	10.0			10.0	9.6	
Total	98.7			97.4	99.7	

*In the wet-chemical analysis, any ZnO is included with MnO.

analyses, normalized to 17 anions and using the H_2O content from the structure analysis are:

IGC29 : $Fe^{2+}_{1.09}Mn^{2+}_{0.77}Zn_{0.06}Ca_{0.05}Fe^{3+}_{3.11}P_{2.99}H_{5.78}O_{17}$

IGC90 : $Fe^{2+}_{1.33}Mn^{2+}_{0.52}Zn_{0.03}Ca_{0.05}Fe^{3+}_{3.03}Al_{0.01}P_{2.97}H_{6.17}O_{17}$.

The simplified formula, based on the crystal structure is $(Fe^{2+},Mn^{2+})_2(Fe^{3+})_3(PO_4)_3(OH)_4(H_2O)$.

8. Crystallography

8.1. X-ray powder diffraction

X-ray powder diffraction data on ground samples were collected at room temperature in the 2θ range 10–140° using a Philips diffractometer employing Co *K*α radiation. The unit-cell parameters were refined using the Rietveld program FULLPROF (Rodriguez-Carvajal, 1990), giving:

$$\text{IGC29}: a = 13.9880(4),\ b = 16.9026(5),\ c = 5.1816(1)\,\text{Å and } V = 1225.1(1)\ \text{Å}^3$$

$$\text{IGC90}: a = 14.0016(5),\ b = 16.8593(5),\ c = 5.1831(1)\text{Å and } V = 1223.5(1)\ \text{Å}^3.$$

The indexed powder pattern (space group *Bbmm*) for IGC29 is given in Table S1 (deposited and freely available as Supplementary Material linked to this article at https://pubs.geoscienceworld.org/eurjmin).

8.2. Neutron powder diffraction

Neutron powder diffraction (NPD) data were collected on ECHIDNA, the high-resolution powder diffractometer at the Open Pool Australian Light (OPAL) water reactor facility at the Australian Nuclear Science and Technology Organisation (Liss *et al.*, 2006). A 5.3 g powdered sample taken from specimen IGC90 was packed in a 9-mm diameter vanadium can and room-temperature data were acquired over 14 h in the 2θ range 5.5°–164°, using a wavelength of 1.6220(5) Å as determined by the La11B6 NIST SRM 660b standard with a step interval of 0.05°. The obtained NPD pattern has a high background due to the large incoherent scattering contribution from hydrogen. A constant value was removed from each point in the pattern to lower the background to a few hundred counts at the lowest point.

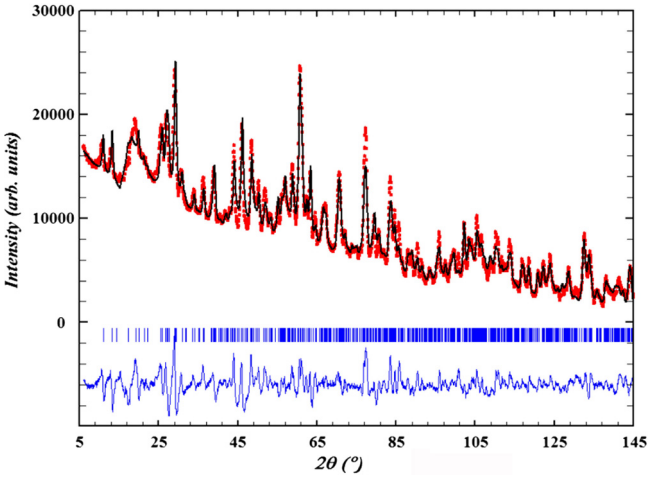

Fig. 7. Rietveld observed (red points) and calculated (black line) neutron-diffraction pattern for ferrorockbridgeite, specimen IGC90. Short bars show the positions of Bragg reflections. Difference plot shown at bottom.

The atomic coordinates for non-hydrogen atoms from the single-crystal refinement were held fixed in the structural refinement using the NPD data with FULLPROF (Rodriguez-Carvajal, 1990), and difference-Fourier maps were used to locate the H atoms. The coordinates and site occupancies of the H atoms were refined, in addition to profile parameters, resulting in convergence at R_{wp} = 8.6%, R_B = 8.5%. The Rietveld profile fitted using the NPD data is shown in Fig. 7. The refined unit-cell parameters are: a = 13.994(1) Å, b = 16.840(1) Å, c = 5.1835(4) Å and

Table 3. Single-crystal X-ray data collection and refinement details for ferrorockbridgeite.

	IGC29	IGC90
Structural formula	$(Mn^{2+}_{0.77}Zn_{0.06}Fe^{2+}_{1.00}Fe^{3+}_{0.17})_{\Sigma 2}$ $Fe^{3+}_3(PO_4)_3(OH)_{4.17}(H_2O)_{0.83}$	$(Mn^{2+}_{0.52}Zn_{0.03}Fe^{2+}_{1.23}Fe^{3+}_{0.22})_{\Sigma 2}$ $Fe^{3+}_3(PO_4)_3(OH)_{4.22}(H_2O)_{0.78}$
Temperature, K	293	100
Wavelength, Å	0.7107 (Mo)	0.7107 (synchrotron)
Space group	*Bbmm*	*Bbmm*
Cell parameters, Å	a = 13.995(1)	a = 14.008(5)
	b = 16.884(1)	b = 16.808(5)
	c = 5.1866(4)	c = 5.190(3)
Volume, Å^3	1225.5	1222.0
Z	4	4
Absorption coefficient	6.21 mm^{-1}	6.38 mm^{-1}
Crystal size, mm	0.085 × 0.075 × 0.007	0.100 × 0.040 × 0.005
Theta range, °	3.15–25	2.42–32.2
Reflections collected	2743	10559
Independent reflections	610 [R_{int} = 0.079]	1020 [R_{int} = 0.043]
Reflections $I > 3\sigma(I)$	470	982
Data completeness	99%	98%
Refinement method	Full-matrix, least squares on F	Full-matrix, least squares on F
Data/restraints/params.	610/0/81	1020/0/82
R indices, $I > 3\sigma(I)$	R_{obs} = 0.048, wR_{obs} = 0.053	R_{obs} = 0.032, wR_{obs} = 0.043
R indices, all data	R_{obs} = 0.066, wR_{obs} = 0.056	R_{obs} = 0.033, wR_{obs} = 0.044
Largest ΔF peaks	+1.09, −1.20 e Å^{-3}	+0.93, −0.78 e Å^{-3}

V = 1221.5 Å^3. The refined H positions are included with the single-crystal refinement data for IGC90 in Table 4.

8.3. Single-crystal studies

A thin platelet of ferrorockbridgeite from specimen IGC29 was used for a single-crystal data collection at ambient temperature on a Rigaku R-Axis Rapid II curved-imaging-plate microdiffractometer utilising monochromatised Mo $K\alpha$ radiation. Diffraction data were collected on a crystal from IGC90 on the microfocus beam line MX2 at the Australian Synchrotron. The collection was made at 100 K using monochromatic radiation with a wavelength of 0.7107 Å. A phi scan was employed over 360° with an exposure time of 36 s. Further details of both data collections are given in Table 3. The synchrotron dataset for IGC90 was obtained to a higher resolution and the structure solution is described for this sample.

A structure model was obtained in space group *Cmcm* by the charge-flipping method using SHELXT (Sheldrick, 2015). The cell and coordinates were transformed to space group *Bbmm*, to be consistent with Moore's (1970) rockbridgeite structure. Initially, the scattering curve for Fe was used for the three metal atom sites, *M*1–*M*3. After refinement, bond valence sums (BVS) were calculated using the parameters of Gagné & Hawthorne (2015) and they indicated that *M*1 and *M*3 were occupied only by Fe^{3+} while *M*2 contained predominantly divalent cations. This agrees with other recent refinements for rockbridgeite-group minerals (Redhammer *et al.*, 2006; Elliott *et al.*, 2009; Röska *et al.*, 2018; Grey *et al.* 2018a). Zn, Mn and Fe were then assigned to *M*2 in amounts corresponding to the EMP analyses. In agreement with Redhammer *et al.* (2006), the small amount of the large Ca^{2+} cation was not incorporated. Its presence is likely due to incipient reaction of the ferrorockbridgeite with Ca-bearing solution, as evidenced by the presence of associated jahnsite and mitridatite.

Refinement with anisotropic displacement parameters in JANA2006 (Petříček *et al.*, 2014) converged at wR_{obs} = 0.043 for 1020 unique reflections. Further details of the refinement are given in Table 3. The refined coordinates, equivalent isotropic displacement parameters and BVS values from the single-crystal refinement are reported in Table 4, together with the results for the H atoms from the NPD refinement.

Refinement of the single-crystal data for a crystal from IGC29 was conducted using the same procedure as described for IGC90. The refinement results are summarised in Table 3. The refined coordinates and isotropic displacement parameters are reported in Table 5. The close agreement between the refined coordinates and isotropic displacement parameters from the two refinements reported in Tables 4 and 5 indicate that no significant structural changes occurred on cooling the sample to 100 K. Polyhedral bond distances and O–H distances are given in Table 6.

9. Discussion

A [001] projection of the structure for ferrorockbridgeite is given in Fig. 8, with all atom sites labelled. The *M*1- and *M*2-centred octahedra form face-sharing trimers, called *h*-clusters by Moore (1970), and these connect into chains along [010] by edge-sharing between the *M*2-centred octahedra. The *M*3 sites comprise corner-connected octahedral dimers that are connected into double columns along [001] by face-sharing. The *M*3–*M*3 separations along [001] are alternately 2.4 and 2.8 Å. The short *M*3–*M*3 distances are

Table 4. Refined coordinates, equivalent isotropic displacement parameters (Å^2) and bond-valence sums (BVS) for ferrorockbridgeite from specimen IGC90. The H atom results are from the NPD refinement of IGC90.

	Occupancy	*x*	*y*	*z*	U_{eq}	BVS
Fe1	1	0	0	0	0.01151(17)	2.92
Fe2	0.72	0.06749(3)	0.15565(3)	0	0.01529(15)	2.18
Mn2	0.26	0.06749(3)	0.15565(3)	0	0.01529(15)	
Zn2	0.02	0.06749(3)	0.15565(3)	0	0.01529(15)	
Fe3	0.5	0.32098(4)	0.13903(3)	0.2300(1)	0.00990(17)	3.01
P1	1	0.14320(4)	0.04404(4)	0.5	0.01064(19)	4.97
P2	1	0.48179(7)	0.25	0	0.0133(3)	4.92
O1	1	0.04516(16)	0.25	0.2562(5)	0.0186(6)	2.00
O2	1	0.08084(10)	0.05792(8)	0.2583(3)	0.0145(4)	2.08
O3	0.5	0.3120(3)	0.25	0.3752(8)	0.0114(10)	1.00
O4	1	0.31690(15)	0.03952(13)	0	0.0226(7)	1.78
O5	1	0.21581(15)	0.17582(13)	0	0.0216(6)	0.91
O6	1	0.42265(13)	0.10466(13)	0.5	0.0137(5)	1.15
O7	1	0.41995(15)	0.17454(13)	0	0.0167(6)	1.89
O8	1	0.22185(13)	0.10815(12)	0.5	0.0113(5)	1.70
H3a	0.76(8)	0.254(3)	0.75	0	0.02	
H3b	0.32(4)	0.198(5)	0.705(5)	0	0.02	
H5a	0.5	0.233(2)	0.157(2)	0.217(6)	0.02	
H5b	0.24(4)	0.233(6)	0.231(4)	0	0.02	
H6	0.5	0.098(2)	0.626(2)	0.158(5)	0.02	

Table 5. Refined coordinates and equivalent isotropic displacement parameters (Å^2) for ferrorockbridgeite from specimen IGC29.

	Occ.	*x*	*y*	*z*	U_{eq}
Fe1	1	0	0	0	0.0145(7)
Fe2	0.585	0.06788(11)	0.15615(9)	0	0.0220(6)
Mn2	0.385	0.06788(11)	0.15615(9)	0	0.0220(6)
Zn2	0.03	0.06788(11)	0.15615(9)	0	0.0220(6)
Fe3	0.5	0.32117(13)	0.13887(11)	0.2308(4)	0.0097(6)
P1	1	0.14287(19)	0.04337(15)	0.5	0.0114(8)
P2	1	0.4823(3)	0.25	0	0.0147(12)
O1	1	0.0452(5)	0.25	0.2540(13)	0.022(2)
O2	1	0.0810(3)	0.0576(3)	0.2600(8)	0.0145(15)
O3	0.5	0.3122(9)	0.25	0.377(2)	0.021(5)
O4	1	0.3193(5)	0.0395(4)	0	0.021(2)
O5	1	0.2171(5)	0.1756(4)	0	0.025(3)
O6	1	0.4223(4)	0.1028(4)	0.5	0.013(2)
O7	1	0.4210(5)	0.1757(4)	0	0.016(2)
O8	1	0.2226(4)	0.1064(4)	0.5	0.013(2)

avoided by half-occupation of the *M*3 site. In space group *Bbmm*, the Fe^{3+} and vacancies are distributed statistically in *M*3, with 50% occupancy of the 16(h) site as shown in Fig. 9. Rockbridgeite-group minerals consistently have broad humps in the powder XRD patterns (shown for IGC29 in Fig. 10) and corresponding diffuse streaked reflections in electron diffraction patterns that violate the *Bbmm* extinction conditions (Grey *et al.*, 2018a). These reflections have been interpreted as resulting from local ordering of the *M*3 cations and vacancies that can be described in space group *Pnma* (Grey *et al.*, 2018a). The *M*3 cation ordering in the *Pnma* model is shown in Fig. 11. A comparison with the disordered model in Fig. 9 shows that the columns of corner-connected *M*3-centred octahedral dimers in the *Bbmm* model are replaced by isolated dimers that lie in (011) planes, thus giving rise to the broad (011) reflection in Fig. 10. Röska *et al.* (2018) also observed weak diffuse streaks in the single-crystal XRD patterns of a rockbridgeite-group mineral that violated the body-centred orthorhombic space-group extinctions. They did not, however, develop a structural model to explain the forbidden reflections and refined the structure in *Cmcm*. In ferrorockbridgeite, the extra reflections are too diffuse to integrate and so only the average structure in *Bbmm* was refined.

The locations of the H atoms are included in Fig. 11. The H atoms are located in the (100) planes containing the *M*3-centred octahedra, and Fig. 11 shows that they are all directed into the unoccupied *M*3-site regions. The H bonding is reported in Table 7. The numbers and positions of the H atoms agree well with those reported by Röska *et al.* (2018), with one notable exception: the latter authors reported the O3 anion to be hydroxyl, whereas we find that

Table 6. Selected interatomic distances [Å] for ferrorockbridgeite (IGC90).

Fe1–O2 (×4)	2.007(1)	Fe3–O3	2.016(2)
Fe1–O6 (×2)	2.066(2)	Fe3–O4	2.056(2)
Av.	2.027	Fe3–O5	1.994(2)
		Fe3–O6	2.080(2)
Fe2–O1 (×2)	2.093(2)	Fe3–O7	1.924(2)
Fe2–O2 (×2)	2.129(2)	Fe3–O8	2.040(2)
Fe2–O5	2.105(2)	Av.	2.018
Fe2–O6	2.202(2)		
Av.	2.125	P2–O1 (×2)	1.546(3)
		P2–O7 (×2)	1.536(2)
P1–O2 (×2)	1.546(2)	Av.	1.541
P1–O4	1.512(2)		
P1–O8	1.541(2)		
Av.	1.536		
		O5–H5A	1.19(4)
O3–H3A	1.13(4)	O5–H5B	0.96(7)
O3–H3B	1.01(6)	O6–H6	0.94(3)

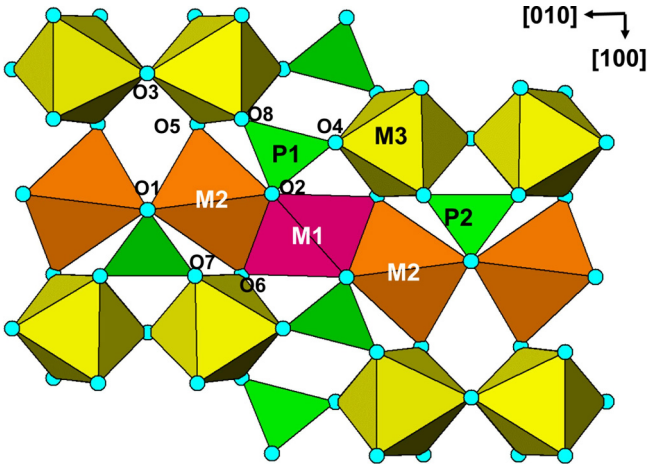

Fig. 8. [001] projection of the ferrorockbridgeite structure.

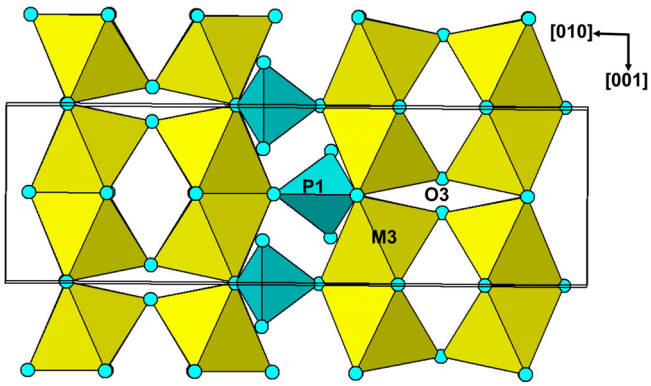

Fig. 9. (100) layer of disordered (50% occupancy) *M*3-centred octahedra in the average structure for ferrorockbridgeite, given in *Bbmm*.

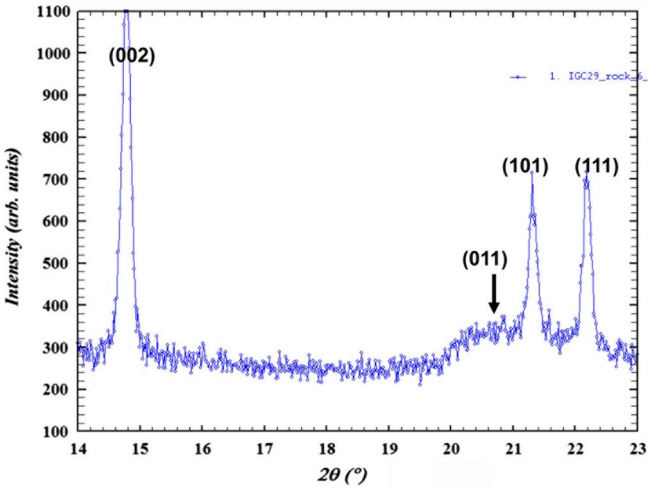

Fig. 10. Low-angle region of powder XRD pattern (Co radiation) for ferrorockbridgeite, specimen IGC29. The broad hump marked by the arrow indexes as (011), forbidden in space group *Bbmm*.

it is a mix of ~70% hydroxyl (O3–H3A) and 30% H_2O (H3B–O3–H3B). Our assignment of the anion O5 as 76% hydroxyl (O5–H5A) plus 24% H_2O (H5A–O5–H5B) and O6 as pure hydroxyl (O6–H6) agrees with the results of Röska *et al*. (2018).

Based on the refined proton site occupancies, the O3 + O5 + O6 anions have the composition $(OH)_{4.22}(H_2O)_{0.78}$ per formula unit (*pfu*). With $3(PO_4)^{3-}$ *pfu* exactly charge-balanced by the three Fe^{3+} in the *M*1 and *M*3 sites, and with the *M*2 site occupied by 0.52 Mn^{2+} + 0.03 Zn + 1.45 Fe, the charge of −4.2 from the hydroxyl ions is balanced by having 1.23Fe^{2+} + 0.22 Fe^{3+} in the *M*2 site. The structural formula is then $(Mn^{2+}_{0.52}Zn_{0.03}Fe^{2+}_{1.23}Fe^{3+}_{0.22})_{\Sigma 2}Fe^{3+}_3(PO_4)_3(OH)_{4.22}(H_2O)_{0.78}$. This gives a somewhat lower overall ferrous-to-ferric ratio, 27.6:72.4 compared to that obtained from Mössbauer spectroscopy, 30.6:69.4. The presence of some Fe^{3+} in the *M*2 site is consistent with the BVS of 2.18 for the site (Table 4). The structural formula can be simplified, when there is no Fe^{3+} in the *M*2 site, to $(Fe^{2+}, Mn^{2+})_2Fe^{3+}_3(PO_4)_3(OH)_4(H_2O)$.

Previous high-quality single-crystal XRD refinements (Redhammer *et al*., 2006; Elliott *et al*., 2009; Grey *et al*., 2018a) failed to unambiguously locate all the H atoms, and Elliott *et al*. (2009) suggested that when high levels of M^{2+} are present as in plimerite, charge balance can be achieved by partial protonation of phosphate anions. Frost *et al*. (2013) identified bands attributed to $PO_3(OH)$ in the Raman spectrum of frondelite and in our study on non-stoichiometric frondelite we included partial protonation of phosphate anions in a general formula (Grey *et al*., 2018a). In the light of the recent NPD studies, that now seems to be unlikely. The replacement of OH^- by H_2O for charge balance when there is greater than one divalent cation in *M*2 has been unambiguously established by Röska *et al*. (2018) using NPD and confirmed in this study in ferrorockbridgeite.

It should be noted that the stoichiometric formula obtained for ferrorockbridgeite does not apply to more oxidized rockbridgeite-group minerals. In our study of a frondelite specimen with 98% of the iron in the ferric form,

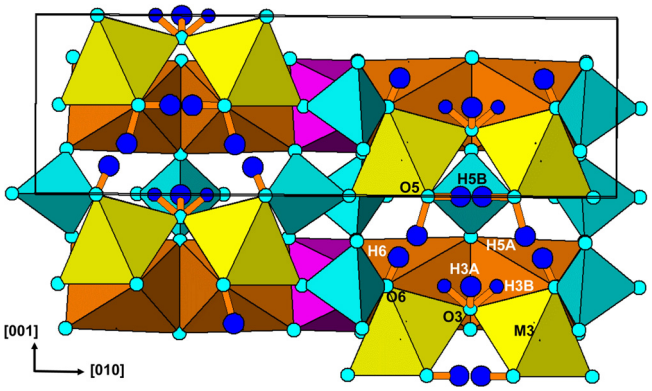

Fig. 11. [100] projection of ferrorockbridgeite structure, showing local ordering of *M*3-centred octahedra in space group *Pnma* (from Grey *et al.*, 2018a) and location of H atoms.

Table 7. Hydrogen bonds for ferrorockbridgeite [Å and °].

D–H...A	*d*(D–H)	*d*(H...A)	*d*(D...A)	<(DHA)
O3–H3B...O8	1.01(6)	1.98(8)	2.775(3)	134(4)
O5–H5A...O8	1.19(3)	1.69(3)	2.835(1)	158(2)
O5–H5B...O5	0.96(7)	1.58(7)	2.494(3)	157(8)
O6–H6...O7	0.94(3)	1.97(3)	2.849(1)	155(2)

we found that the iron oxidation is accompanied by selective leaching of iron from the *M*2 site, resulting in up to 17% vacancies in *M*2 (Grey *et al.*, 2018a). We are currently studying a range of oxidized rockbridgeite-group minerals, including the type frondelite and rockbridgeite specimens, to establish a general formula that applies to non-stoichiometric, oxidized members.

Acknowledgements: This research was undertaken in part using the MX2 beamline at the Australian Synchrotron, part of ANSTO, and made use of the Australian Cancer Research Foundation (ACRF) detector. We acknowledge the Diffraction Laboratory at CSIRO Mineral Resources, Clayton, for use of their Panalytical Empyrean powder XRD diffractometer. Thanks to Cameron Davidson for preparing sample mounts for EMP analyses and for SEM, and to James Hester for starting the data collection on ECHIDNA.

References

Elliott, P., Kolitsch, U., Giester, G., Libowitzky, E., McCammon, C., Pring, A., Birch, W.D., Brugger, J. (2009): Description and crystal structure of a new mineral–plimerite, $ZnFe_4^{3+}(PO_4)_3(OH)_5$ – the Zn-analogue of rockbridgeite and frondelite, from Broken Hill, New South Wales, Australia. *Mineral. Mag.*, **73**, 131–148.

Frondel, C. (1949): The dufrenite problem. *Am. Mineral.*, **34**, 513–540.

Frost, R.L., Xi, Y., Scholz, R., Belotti, F.M., Beganovic, M. (2013): SEM-EDX, Raman and infrared spectroscopic characterization of the phosphate mineral frondelite $(Mn^{2+})(Fe^{3+})_4(PO_4)_3(OH)_5$. *Spectrochim. Acta*, **A110**, 7–13.

Gagné, O.C. & Hawthorne, F.C. (2015): Comprehensive derivation of bond-valence parameters for ion pairs involving oxygen. *Acta Crystallogr.*, **B71**, 562–578.

Grey, I.E., Williams, T., Kampf, A.R., Cashion, J.D., Gozukara, Y., MacRae, C.M., Keck, E. (2018a): Non-stoichiometry and local order in minerals with the rockbridgeite structure. *Eur. J. Mineral.*, **30**, 773–783.

Grey, I.E., Kampf, A.R., Keck, E., MacRae, C.M., Cashion, J.D., Gozukara, Y. (2018b): Ferrorockbridgeite, IMA 2018–004. CNMNC Newsletter No. 43, June 2018, page 649. *Eur. J. Mineral.*, **30**, 647–652.

Gunter, M.E., Bandli, B.R., Bloss, F.D., Evans, S.H., Su, S.C., Weaver, R. (2004): Results from a McCrone spindle stage short course, a new version of EXCALIBR, and how to build a spindle stage. *The Microscope*, **52**, 23–39.

Lindberg, M.L. (1949): Frondelite and the frondelite-rockbridgeite series. *Am. Mineral.*, **34**, 541–549.

Liss, K.-D., Hunter, B.A., Hagen, M.E., Noakes, T.J., Kennedy, S.J. (2006): ECHIDNA – the new high-resolution powder diffractometer being built at OPAL. *Physica B*, **385–386**, 1010–1012.

Mandarino, J.A. (1981): The Gladstone-Dale relationship: Part IV. The compatibility concept and its application. *Can. Mineral.*, **19**, 441–450.

Moore, P.B. (1970): Crystal chemistry of the basic iron phosphates. *Am. Mineral.*, **55**, 135–169.

Mücke, A. (1981): The paragenesis of the phosphate minerals of the Hagendorf pegmatite – a general view. *Chemie der Erde*, **40**, 217–234.

Nasdala, L., Kronz, A., Wirth, R., Vaczi, T., Perez-Soba, C., Willner, A., Kennedy, A.K. (2009): The phenomenon of deficient electron microprobe totals in radiation-damaged and altered zircon. *Geochim. Cosmochim. Acta*, **73**, 1637–1650.

Petříček, V., Dušek, M., Palatinus, L. (2014): Crystallographic Computing System JANA2006: General features. *Z. Kristallogr.*, **229**, 345–352.

Redhammer, G.J., Roth, G., Tippelt, G., Bernroider, M., Lottermoser, W., Amthauer, G., Hochleitner, R. (2006): Manganoan rockbridgeite; structure analysis and ^{57}Fe Mössbauer spectroscopy. *Acta Crystallogr.*, **C62**, i24–i28.

Rodriguez-Carvajal, J. (1990): FULLPROF: a program for Rietveld refinement and pattern matching analysis, *in:* Proceedings of the Satellite Meeting on Powder Diffraction of the XV Congress of the IUCr, Toulouse, France.

Röska, B., Park, S.-H., Behal, D., Hess, K.-U., Günther, A., Benka, G., Pfleiderer, C., Hoezel, M., Kimura, T. (2018): Determination of the hydrogen-bond network and the ferromagnetic structure of a rockbridgeite-type compound. $Fe^{2+}Fe_{3.2}^{3+}(Mn^{2+}, Zn)_{0.8}(PO_4)_3(OH)_{4.2}(HOH)_{0.8}$. *J. Phys. Condens. Matter*, **30**, 235401.

Sejkora, J., Plasil, J., Filip, J. (2011): Plimerite from Krasno near Horni Slavkov ore district, Czech Republic. *J. Geosci.*, **56**, 215–229.

Sheldrick, G.M. (2015): Crystal structure refinement with SHELXL. *Acta Crystallogr.*, **C71**, 3–8.

Received 21 August 2018
Modified version received 17 October 2018
Accepted 18 October 2018